MITRE TECHNICAL REPORT

Evaluating Detection and Estimation Capabilities of Magnetometer-Based Vehicle Sensors

May 2012

Dr. David M. Slater and Dr. Garry M. Jacyna

Sponsor:	Corporate Initiative	**Contract No.:**	W15P7T-13-C-F600
Div. No.:	E520, E400	**Project No.:**	01CCG020-A8

Corporate Headquarters
McLean, Virginia

Report Documentation Page

Form Approved
OMB No. 0704-0188

1. REPORT DATE	2. REPORT TYPE	3. DATES COVERED
MAY 2012		**00-00-2012 to 00-00-2012**

4. TITLE AND SUBTITLE	5a. CONTRACT NUMBER
Evaluating Detection and Estimation Capabilities of Magnetometer-Based Vehicle Sensors	5b. GRANT NUMBER
	5c. PROGRAM ELEMENT NUMBER
6. AUTHOR(S)	5d. PROJECT NUMBER
	5e. TASK NUMBER
	5f. WORK UNIT NUMBER
7. PERFORMING ORGANIZATION NAME(S) AND ADDRESS(ES) **MITRE Corporation,7525 Colshire Drive ,McLean,VA,22102**	8. PERFORMING ORGANIZATION REPORT NUMBER
9. SPONSORING/MONITORING AGENCY NAME(S) AND ADDRESS(ES)	10. SPONSOR/MONITOR'S ACRONYM(S)
	11. SPONSOR/MONITOR'S REPORT NUMBER(S)

12. DISTRIBUTION/AVAILABILITY STATEMENT
Approved for public release; distribution unlimited

13. SUPPLEMENTARY NOTES
sponsored by NSA.

14. ABSTRACT

In an effort to secure the northern and southern United States borders, MITRE has been tasked with developing Modeling and Simulation (M&S) tools that accurately capture the mapping between algorithm-level Measures of Performance (MOP) and system-level Measures of Effectiveness (MOE) for current/future surveillance systems deployed by the the Customs and Border Protection Office of Technology Innovations and Acquisitions (OTIA). This analysis is part of a larger M&S undertaking. The focus is on two MOPs for magnetometer-based Unattended Ground Sensors (UGS).UGSare placed near roads to detect passing vehicles and estimate properties of the vehicle?s trajectory such as bearing and speed. The first MOP considered is the probability of detection. We derive probabilities of detection for a network of sensors over an arbitrary number of observation periods and explore how the probability of detection changes when multiple sensors are employed. The performance of UGS is also evaluated based on the level of variance in the estimation of trajectory parameters. We derive the Cram?r-Rao bounds for the variances of the estimated parameters in two cases: when no a priori information is known and when the parameters are assumed to be Gaussian with known variances. Sample results show that UGS perform significantly better in the latter case.

15. SUBJECT TERMS

16. SECURITY CLASSIFICATION OF:			17. LIMITATION OF ABSTRACT	18. NUMBER OF PAGES	19a. NAME OF RESPONSIBLE PERSON
a. REPORT **unclassified**	b. ABSTRACT **unclassified**	c. THIS PAGE **unclassified**	**Same as Report (SAR)**	**19**	

MITRE Project Approval: _____

Dr. Garry Jacyna

Abstract

In an effort to secure the northern and southern United States borders, MITRE has been tasked with developing Modeling and Simulation (M&S) tools that accurately capture the mapping between algorithm-level Measures of Performance (MOP) and system-level Measures of Effectiveness (MOE) for current/future surveillance systems deployed by the the Customs and Border Protection Office of Technology Innovations and Acquisitions (OTIA). This analysis is part of a larger M&S undertaking. The focus is on two MOPs for magnetometer-based Unattended Ground Sensors (UGS). UGS are placed near roads to detect passing vehicles and estimate properties of the vehicle's trajectory such as bearing and speed. The first MOP considered is the probability of detection. We derive probabilities of detection for a network of sensors over an arbitrary number of observation periods and explore how the probability of detection changes when multiple sensors are employed. The performance of UGS is also evaluated based on the level of variance in the estimation of trajectory parameters. We derive the Cramér-Rao bounds for the variances of the estimated parameters in two cases: when no a priori information is known and when the parameters are assumed to be Gaussian with known variances. Sample results show that UGS perform significantly better in the latter case.

1 Introduction

As part of the sensor package deployed by the Customs and Border Protection Office of Technology Innovation and Acquisitions (OTIA), Unattended Ground Sensors (UGS) monitor and report on vehicle traffic in remote areas that are unaccessible to radio, electro-optical and infrared sensors. This analysis focuses on vehicle traffic using two-axis fluxgate magnetometers whose operating characteristics are well documented [1, 2]. Such magnetometers measure two perpendicular magnetic components of the external field. When a motorized ground vehicle passes relatively close to the sensor ($\lesssim 40$ m), the vehicle exhibits a magnetic moment because it is (traditionally) comprised of nontrivial quantities of magnetic materials. At ranges much greater than its size, the vehicle behaves like a magnetic dipole and thus can be modeled as such. The magnetometer measures the magnetic field components of the dipole, from which it determines if a vehicle is present and then estimates its position, velocity, and magnetic moments.

This analysis is part of a larger Modeling and Simulation effort to estimate algorithm-level Measures of Performance (MOP) and map them to system-level Measures of Effectiveness (MOE). We concentrate on two MOPs: probability of detection and variance in trajectory estimation. The probability of detection for a single magnetometer was derived by Jacyna and Christou [3]. We extend this work to include a network of magnetometers as well as detection over multiple observation periods. The performance of UGSs are also evaluated based on the level of variance in the estimation of the vehicle's heading, position, and magnetic moments. Two cases are considered. First, the parameters are assumed to be unknown random variables; next, they are assumed to be Gaussian random variables with a priori known variances. Lower bounds on the variances for all parameters are derived in both cases.

The report is organized as follows. The vehicle model is formulated in Section 2. The vehicle is assumed to move with constant velocity over an observation period (< 1 sec); it is modeled as a prolate homogeneous ellipsoid of revolution that behaves like a magnetic dipole. Next, the probability of detection for a network of UGS over an arbitrary number of observation periods is computed in section 3. In section 4, the Cramér-Rao bounds for the variances of the estimation parameters are derived for the two cases described above. The bounds for the variances are also found for the general case where some parameters may be completely unknown, others may be known exactly, and the rest are assumed to be Gaussian with some known variance. Lastly, section 5 contains sample UGS evaluation scenarios. The probability of detection for a set of five magnetometers is compared with a single magnetometer. Further, we show that the probability of detection can be raised from 60% (one observation period) to nearly unity by considering the overall probability of detection over multiple observation periods. Next, bounds on the variances

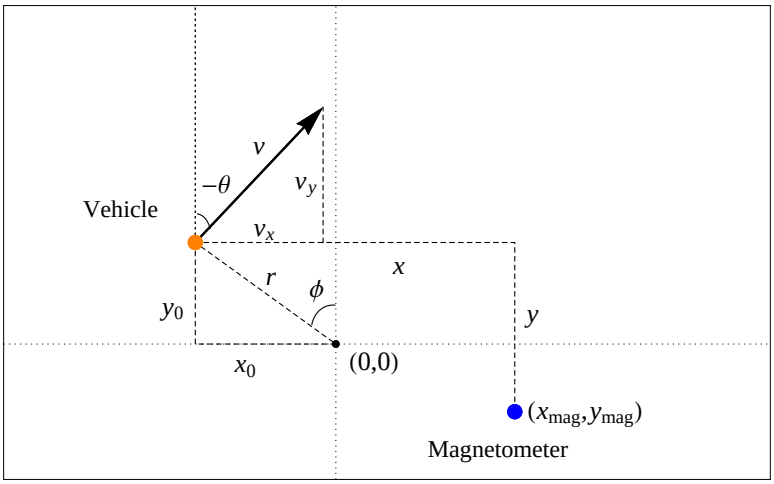

Figure 1: Schematic of a vehicle moving past a magnetometer

of parameters are calculated for a vehicle passing a magnetometer. It is shown that by assuming the parameters are Gaussian random variables with plausible variances, the estimation quality is much better than when the parameters are unknown random variables. The effect of velocity on estimation performance is also explored.

2 Model Formulation

Consider a vehicle traveling with velocity v near an UGS. Over sufficiently short observation periods, one can assume the vehicle moves in a straight line with constant speed. In particular, if $(x, y) = (x_0 - x_m, y_0 - y_m)$ is the position of the vehicle relative to the sensor at time t_0, then its positions over an observation period T are $(x_k, y_k) = (x + ktv_x, y + ktv_y)$, for $k \in (0, N)$, where $N = 2bT$, $t = 1/(2b)$, and b is the sensor bandwidth.

As the UGS utilize two-axis magnetometers, one must compute the magnetic field components of the vehicle in the longitudinal and transverse directions. For this calculation, the vehicle's shape is approximated as a prolate homogeneous ellipsoid of revolution with axes $A \geq B = C$. Such an approximation is viewed as a reasonable approximation for a variety of vehicle types[4]. The induced moments of the vehicle are derived by Christou and Jacyna[3] based on work by Osborn[5] and Jackson[6]. They determine the magnetic field components of

the dipole to be[6]:

$$B_1 = 10^{-7}\frac{M_1(3x^2 - R^2) + 3M_2xy}{R^5} \text{ (teslas)} \tag{1}$$

$$B_2 = 10^{-7}\frac{M_2(3y^2 - R^2) + 3M_1xy}{R^5} \text{ (teslas)}, \tag{2}$$

where $\mathbf{M} = (M_1, M_2)$ is the induced moment of vehicle, R is the range from the sensor, and (x, y) is the position of the vehicle relative to the sensor. The induced moment of the vehicle is a function of vehicle, location and trajectory characteristics. The derivation of $\mathbf{M}$ may be found in Appendix A.

3 Detection

To determine the probability of detection, a matched filter is used to compute the deflection ratio d[3]. The calculation details may be found in Appendix B. The probability of detection (PD) and the probability of a false alarm (PFA) for a single magnetometer over one observation period are

$$PFA = \Phi(\eta) \tag{3}$$

$$PD = \Phi(\eta - d), \tag{4}$$

where Φ is the modified complimentary error function [1] and η is a threshold. In order to find the probability of detection, equation (3) is solved for η and the resulting value is substituted into equation (4).

In general, we are interested in the case of n magnetometers and K observation periods. First consider the case of a single observation period. Let $(\mathbf{x}_{mag}, \mathbf{y}_{mag})$ be the positions of the sensors. Then the positions of the vehicle at the start of the observation period relative to the n sensors are $(\mathbf{x}, \mathbf{y}) = (x_0 - \mathbf{x}_{mag}, y_0 - \mathbf{y}_{mag}) \in \mathbb{R}_{2,n}$. Then, the probability that sensor j detects the vehicle, PD_j, is given by equation (4). Assuming magnetometer measurements are independent, the probability that **at least one** sensor detects the vehicle during the observation period is

$$p(D > 0) = 1 - \prod_{j=1}^{n}(1 - PD_j). \tag{5}$$

[1] The modified complimentary error function is $c(x) = \frac{1}{\sqrt{2\pi}}\int_x^\infty e^{-t^2/2}dt$

Multiple observation periods may be handled in the same manner. Let $PD_{j,k}$ be the probability sensor j detects the vehicle during observation period k. Then, assuming the observation periods are independent, the probability of detection over K observation periods using n magnetometers is

$$p(D > 0) = 1 - \prod_{j=1}^{n} \prod_{k=1}^{K} (1 - PD_{j,k}). \tag{6}$$

4 Bounds on Variance in Parameter Estimation

Now consider a scenario in which one or more UGS are used to estimate a vehicle's trajectory such as position and velocity. In this case, we want to determine bounds for the estimation variance; this is achieved by calculating the Cramér-Rao bound on the covariance matrix[7]. The Cramér-Rao bound is derived for the cases where there is no a priori knowledge of the parameters and when the parameters are assumed to be Gaussian random variables with known variances.

4.1 Setup

Let $\mathbf{B} = \{B_k\}, k = 0, \ldots N-1$, be a set of sample magnetic field components for a single sensor. Then define $r_k = B_k + n_k$ to be the signal at the magnetometer, where $\{n_k\}$ is zero-mean independent Gaussian $1/f$ noise. where $\{n_k\}$ is zero-mean Gaussian $1/f$ noise. Without loss of generality, it is assumed that $\{n_k\}$ is statistically independent for this analysis. By assumption, the vehicle moves in a straight line with constant speed over an observation period. Hence, the parameters to be estimated (see Figure 1) are $\mathbf{z} = (x_0, y_0, v, \theta, M_1, M_2)$, or equivalently, $\mathbf{w} = (r, \phi, v_x, v_y, M_1, M_2)$. We will compute the covariance matrix for the first set of parameters and use a transformation to obtain the second set. The positions of the vehicle over the observation period are

$$x_k = (x_0 - x_m) - ktv \sin\theta \tag{7}$$

$$y_k = (y_0 - y_m) + ktv \cos\theta, \tag{8}$$

where $t = T/N$ is the fixed time between measurements.

4.2 Cramér-Rao Bound: No a priori information

To estimate $\mathbf{z}$ when no a priori information exists, one uses the maximum likelihood estimator

$$\hat{\mathbf{z}} \Leftarrow \max_{\mathbf{z}} p(\mathbf{r}|\mathbf{z}). \tag{9}$$

We now compute $p(\mathbf{r}|\mathbf{z})$. Let r_k^j and B_k^j denote the components of r_k and B_k, respectively $(j = 1, 2)$. B_k^j can be written as a function of $\mathbf{z}$ and k because

$$B_k^j = B_k^j(x_0 - x_m - ktv\sin\theta, y_0 - y_m + ktv\cos\theta) = B^j(\mathbf{z}, k). \tag{10}$$

Then, since r_k^j is Gaussian with variance σ,

$$p(\mathbf{r}|\mathbf{z})) = \prod_{j=1}^{2}\prod_{k=0}^{N-1} \frac{1}{\sqrt{2\pi\sigma^2}} \exp\left[-\frac{(r_k^j - B^j(\mathbf{z}, k))^2}{2\sigma^2}\right]. \tag{11}$$

Note that if we wanted to compute the minimizer, we would take the four derivatives of $p(\mathbf{r}|\mathbf{z})$ and solve for (x_0, y_0, v, θ) as functions of $\mathbf{r}$; however, our interest is in evaluating the estimator using the Cramér-Rao Bound $CR(\mathbf{z})$:

$$Cov\{\mathbf{z}(\mathbf{r})\} \geq \left[\mathbf{I} + \frac{\partial \mathbf{b}(\mathbf{z})}{\partial \mathbf{z}}\right]^T \mathcal{F}_{mle}^{-1}(\mathbf{z}) \left[\mathbf{I} + \frac{\partial \mathbf{b}(\mathbf{z})}{\partial \mathbf{z}}\right] \triangleq CR(\mathbf{z}), \tag{12}$$

where $\mathbf{b}$ is the bias of the estimator and $\mathcal{F}_{mle}$ the Fisher information matrix:

$$\mathcal{F}_{mle} = -\mathcal{E}\left[\frac{\partial^2}{\partial \mathbf{z}^2}\left\{\ln p(\mathbf{r}|\mathbf{z})\right\}\right]. \tag{13}$$

Assuming the estimator is unbiased, the Cramér-Rao Bound is $\mathcal{F}_{mle}^{-1}$. In this case, the first component of $\mathcal{F}_{mle}$ can be computed by evaluating

$$\frac{\partial^2}{\partial x_0^2}\left[\ln p(\mathbf{r}|\mathbf{z})\right] = \frac{1}{\sigma^2}\sum_{i=1}^{2}\left[\sum_{k=0}^{N-1}\frac{\partial^2 B^i(\mathbf{z}, k)}{\partial x_0^2} r_k^i - \left(\frac{\partial B^i(\mathbf{z}, k)}{\partial x_0}\right)^2 - B^i(\mathbf{z}, k)\frac{\partial^2 B^i(\mathbf{z}, k)}{\partial x_0^2}\right] \tag{14}$$

and noting that the only non-constant quantity is r_k^i, which has mean $B_k^i(\mathbf{z}, k)$. Thus,

$$\mathcal{E}\left[\frac{\partial^2}{\partial x_0^2}\left[\ln p(\mathbf{r}|\mathbf{z})\right]\right] = \frac{1}{\sigma^2}\sum_{i=1}^{2}\sum_{k=0}^{N-1}\frac{\partial^2 B^i(\mathbf{x},k)}{\partial x_0^2}\mathcal{E}\left[r_k^i\right] - \left(\frac{\partial B^i(\mathbf{z},k)}{\partial x_0}\right)^2 - B^i(\mathbf{z},k)\frac{\partial^2 B^i(\mathbf{z},k)}{\partial x_0^2} \tag{15}$$

$$= -\frac{1}{\sigma^2}\sum_{i=1}^{2}\sum_{k=0}^{N-1}\left(\frac{\partial B^i(\mathbf{z},k)}{\partial x_0}\right)^2. \tag{16}$$

The other components of $\mathcal{F}_{mle}$ are computed similarly. In general, the (a, b) component is

$$-\mathcal{E}\left[\frac{\partial^2}{\partial z_a \partial z_b}\left[\ln p(\mathbf{r}|\mathbf{z})\right]\right] = \frac{1}{\sigma^2}\sum_{i=1}^{2}\sum_{k=0}^{N-1}\left(\frac{\partial B^i(\mathbf{z},k)}{\partial z_a}\right)\left(\frac{\partial B^i(\mathbf{z},k)}{\partial z_b}\right). \tag{17}$$

Thus, the Cramér-Rao bound on the covariance matrix is

$$Cov(\mathbf{z}) \geq \left[\frac{1}{\sigma^2}\sum_{i=1}^{2}\sum_{k=0}^{N-1}\left(\frac{\partial}{\partial \mathbf{z}}B^i(\mathbf{z},k)\right)\otimes\left(\frac{\partial}{\partial \mathbf{z}}B^i(\mathbf{z},k)\right)\right]^{-1} = CR(\mathbf{z}) \tag{18}$$

where $\otimes$ represents the outer product of the two vectors.

We also seek to bound the variance with respect to $\mathbf{w} = (r, \phi, v_x, v_y, M_1, M_2)$. The bound is computed from $CR(\mathbf{z})$ using the Jacobian of the transformation $\mathbf{J}$:

$$CR(\mathbf{w}) = \mathbf{J}CR(\mathbf{z})\mathbf{J}^T. \tag{19}$$

The Jacobian has components $J_{ij} = \frac{dw_i}{dz_j}$ and may be written as

$$\mathbf{J} = \begin{pmatrix} x/r & y/r & 0 & 0 & 0 & 0 \\ -y/r^2 & -x/r^2 & 0 & 0 & 0 & 0 \\ 0 & 0 & -\sin\theta & -v\cos\theta & 0 & 0 \\ 0 & 0 & \cos\theta & -v\sin\theta & 0 & 0 \\ 0 & 0 & 0 & 0 & 1 & 0 \\ 0 & 0 & 0 & 0 & 0 & 1 \end{pmatrix}. \tag{20}$$

4.3 Cramér-Rao Bound: with a priori information

Now suppose we have a priori information about $\mathbf{z} = (x_0, y_0, v, \theta, M_1, M_2)$. In particular, suppose the parameters are independent Gaussian random variables (note that the magnetic

moments may be treated as Gaussian as the vehicle is approximated by an ellipsoid) with standard deviations $\boldsymbol{\sigma} = (\sigma_{x_0}, \sigma_{y_0}, \sigma_v, \sigma_\theta, \sigma_{M_1}, \sigma_{M_2})$; the magnetic moments may be treated as Gaussian as the vehicle is approximated by an ellipsoid. The desired estimator is the maximum a posteriori estimator

$$\hat{\mathbf{z}} \Rightarrow \max_{\mathbf{z}} p(\mathbf{z}|\mathbf{r}) = \max_{\mathbf{z}} \frac{p(\mathbf{r}|\mathbf{z})p(\mathbf{z})}{p(\mathbf{r})}. \tag{21}$$

To evaluate this estimator we proceed as in the last section: compute the Cramér-Rao bound under the assumption that there is no bias

$$Cov(\mathbf{z}) = \mathcal{F}_{post}^{-1}. \tag{22}$$

Now, the Fisher information matrix is

$$\mathcal{F}_{\text{post}} = -\mathcal{E}\left[\frac{\partial^2}{\partial \mathbf{z}^2}\left[\ln \frac{p(\mathbf{r}|\mathbf{z})p(\mathbf{z})}{p(\mathbf{r})}\right]\right] \tag{23}$$

$$= -\mathcal{E}\left[\frac{\partial^2}{\partial \mathbf{z}^2}\left[\ln p(\mathbf{r}|\mathbf{z}) + \ln p(\mathbf{z}) - p(\mathbf{r})\right]\right] \tag{24}$$

$$= \mathcal{F}_{\text{mle}} - \mathcal{E}\frac{\partial^2}{\partial \mathbf{z}^2}\left[\ln p(\mathbf{z})\right]. \tag{25}$$

Next, since the parameters are independent normally distributed random variables,

$$p(\mathbf{z}) = \prod_{i=1}^{4} \frac{1}{\sqrt{2\pi\sigma_i^2}} \exp\left[-\frac{(z_i - \mu_i)^2}{2\sigma_i^2}\right], \tag{26}$$

which implies that

$$\frac{\partial}{\partial z_i}\frac{\partial}{\partial z_j}\left[\ln p(\mathbf{z})\right] = \begin{cases} 0 & : \text{if } i \neq j \\ -1/\sigma_i^2 & : \text{if } i = j \end{cases}. \tag{27}$$

Thus,

$$\mathcal{F}_{post} = \mathcal{F}_{mle} + \text{diag}(1/\sigma_1^2, \ldots 1/\sigma_6^2), \tag{28}$$

where $\text{diag}(1/\sigma_1^2, \ldots 1/\sigma_6^2)$ represents a diagonal matrix with diagonal elements $1/\sigma_i^2$.

If any of the variances tend to infinity, this corresponds to no a priori knowledge of that parameter. Indeed, if all variances are infinity, $\mathcal{F}_{post} = \mathcal{F}_{mle}$, as expected. Alternatively, if a

variance tends toward zero, this represents having complete knowledge of that parameter. Hence, the derived framework may be used in cases where some parameters are known exactly, some whose variance may be bounded, and some for which we have no information.

4.4 Multiple Sensors and Multiple Observation Periods

As we did in section 3, the estimation framework can be generalized to multiple sensors over multiple observation periods. First consider the case of n magnetometers, a single observation period with N samples, and no a priori information. Then, as in section 3, the positions of the vehicle at the start of an observation period are $(\mathbf{x}, \mathbf{y}) = (x_0 - \mathbf{x}_m, y_0 - \mathbf{y}_m)$. Let $\mathbf{R} = [\mathbf{r}_1, \mathbf{r}_2, \dots \mathbf{r}_n] \in \mathbb{R}_{N,n}$, where $\mathbf{r}_j$ is the signal at the j^{th} magnetometer. Now, assuming the magnetometers are independent, the maximum likelihood estimator is

$$\hat{\mathbf{z}} \Leftarrow \max_{\mathbf{z}} p(\mathbf{R}|\mathbf{z}) = \max_{\mathbf{z}} \prod_{j=1}^{n} p(\mathbf{r}_j|\mathbf{z}). \tag{29}$$

Let $B_j^1(\mathbf{z}, k)$ and $B_j^2(\mathbf{z}, k)$ denote the magnetic field components for the j^{th} sensor. It is then straightforward to show that the Cramér-Rao bound is

$$Cov(\mathbf{z}) \geq \left[\frac{1}{\sigma^2} \sum_{j=1}^{n} \sum_{i=1}^{2} \sum_{s=0}^{N-1} \left(\frac{\partial}{\partial \mathbf{z}} B_j^i(\mathbf{z}, s) \right) \otimes \left(\frac{\partial}{\partial \mathbf{z}} B_j^i(\mathbf{z}, s) \right) \right]^{-1} = \mathcal{F}_{mle}^{-1} = CR(\mathbf{z}), \tag{30}$$

where $\otimes$ represents the Kronecker product. Next let there be K observation periods and let $B_j^{1,k}$ and $B_j^{2,k}$ be the magnetic field components for the j^{th} sensor during the k^{th} observation period. Then

$$Cov(\mathbf{z}) \geq \left[\frac{1}{\sigma^2} \sum_{k=1}^{K} \sum_{j=1}^{n} \sum_{i=1}^{2} \sum_{s=0}^{N-1} \left(\frac{\partial}{\partial \mathbf{z}} B_j^{i,k}(\mathbf{z}, s) \right) \otimes \left(\frac{\partial}{\partial \mathbf{z}} B_j^{i,k}(\mathbf{z}, s) \right) \right]^{-1} = \mathcal{F}_{mle}^{-1} = CR(\mathbf{z}). \tag{31}$$

Finally, when parameters are assumed to be Gaussian with standard deviations $(\sigma_1, \dots, \sigma_6)$,

$$Cov(\mathbf{z})_{post} \geq \left[\mathcal{F}_{mle} + \text{diag}(1/\sigma_1^2, \dots, 1/\sigma_6^2) \right]^{-1} = \mathcal{F}_{post}^{-1} = CR(\mathbf{z}). \tag{32}$$

Light vehicle dimensions	$l = 4m, w = 2m, h = 2m$
ATV dimensions	$l = 2m, w = 1.2m, h = 1.2m$
Magnetic inclination angle (Tucson, AZ)	$59°$
Magnetic declination angle (Tucson, AZ)	$-11°$
Magnetic field (Tucson, AZ)	57 μTesla
Material magnetic susceptibility	10
Noise spectral level	100 pTesla/sqrt(Hz)
High-pass filter cut-off	3 Hz
Magnetometer bandwidth	11 Hz
Magnetometer sensitivity	9×10^{-10} Tesla
False Alarm Probability (PFA)	1×10^{-6}

Table 1: Detection Simulation Parameters

5 Sample Results

Probabilities of detection and bounds on the kinematic variances are computed for light vehicles (cars) and off road vehicles (ATVs). Table 1 summarizes the parameters used in the simulations. For the following calculations, the magnetometer observation time interval and the overall time interval were both taken to be 0.5 sec.

5.1 Detection Results

Figure 2 displays a scenario in which a vehicle (either a car or an ATV) passes a single magnetometer placed near a roadway. The distance from the middle of the road to the magnetometer is the closest point of approach (CPA). The magnetometer attempts to detect the vehicle twice

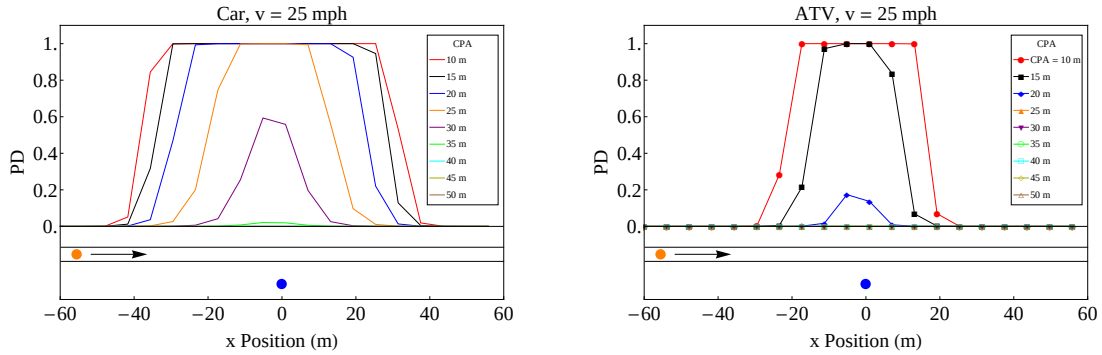

Figure 2: Detection Probabilities for a car and an ATV traveling at 25 mph passing a single magnetometer for various closest points of arrival (CPA).

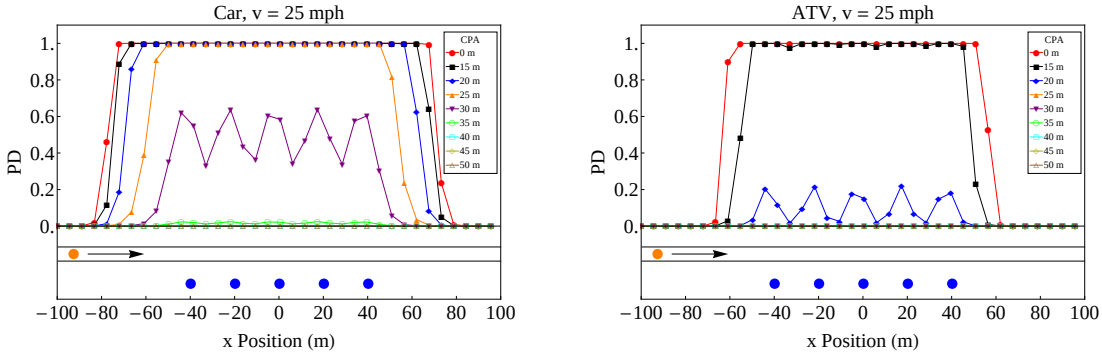

Figure 3: Detection Probabilities for a car and an ATV traveling at 25 mph passing a set of five magnetometers for various closest points of arrival.

a second; the probability of detection over each observation interval is displayed relative to the position of the vehicle at the start of the interval. For the car, the sensor will almost always detect the vehicle at least once provided the sensor is placed within 25m of the road, while if it is placed further than 35m from the road the sensor almost always fails to detect the vehicle. The ATV displays similar results although that the magnetometer must be placed within 10m of the road for a high probability of detection; this is due to the size of the ATV. Being significantly smaller, the ATV has a weaker magnetic field.

In figure 3, five magnetometers are placed 20m apart along the road. When the CPA is 30m, there is an interval where, as the car travels along the road, each magnetometer has a nontrivial probability of detecting the vehicle. For the parameters used, the magnetometers are spaced sufficiently far apart that, in general, at any given time only one magnetometer is contributing significantly to the probability of detection. Likewise, the probability of detection for the ATV is similar for a CPA of 20m.

Another case of interest is the probability that a vehicle is detected by at least one magnetometer during any of the observation periods; this is shown in Figure 4, where the dots are the points calculated in Figures 2 and 3. By adding four more magnetometers, we greatly increase the probability of detection over the intermediate range. For example, consider a car and a single magnetometer with a CPA of 30m. The maximum probability of detection over a single observation period is 59.3%, while the probability that it is detected at least once is 90%. Further, when the single magnetometer is replaced by an array of five, the probability of detection is nearly one.

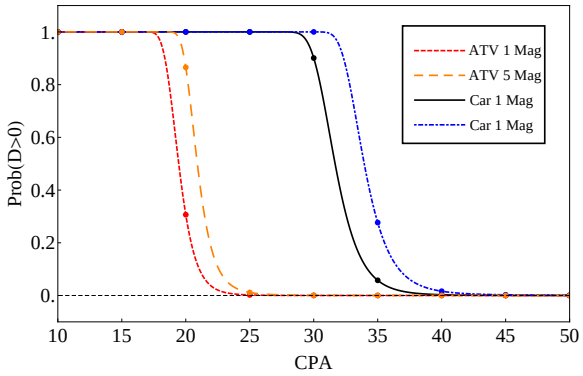

Figure 4: Probabilities that a car or an ATV is detected at least once by a magnetometer as a function of the closest point of arrival (CPA).

5.2 Estimation Results

Recall that the Cramér-Rao bound is the minimum variance for an efficient estimator. We consider two cases. First, no information is known about the parameters to be estimated and the Cramér-Rao bound is given by equation (18). In the second case, we assume the parameters $\mathbf{z} = (x_0, y_0, v, \theta, M_1, M_2)$ are Gaussian random variables with standard deviations given in Table 2.

Let us revisit the scenario of a vehicle passing a single magnetometer with a fixed speed of 25 mph. Figure 5 shows a log plot of the lower bounds on the standard deviations of the parameters $(x_0, y_0, v, \theta, M_1, M_2)$ in each case. In either case, note that, for positions to the left of the sensor, the bound on the stand deviation is low for the parameters x_0, y_0, v, and θ; with no a priori information the bounds quickly grow so that any estimate is worthless. Witha priori information, curves are bounded above by the a priori standard deviations. This can be observed for σ_θ where the curve asymptotes to the a priori standard deviation (e.g., the dashed orange curve at 15 degrees). Because the Cramér-Rao bound is a *lower* bound on the variance, to

Variable	A priori standard deviation
x_0	30 m
y_0	5 m
v	10 mph
θ	15 degrees
M_1	100 ampere-m^2
M_2	100 amperem^2

Table 2: A priori standard deviations

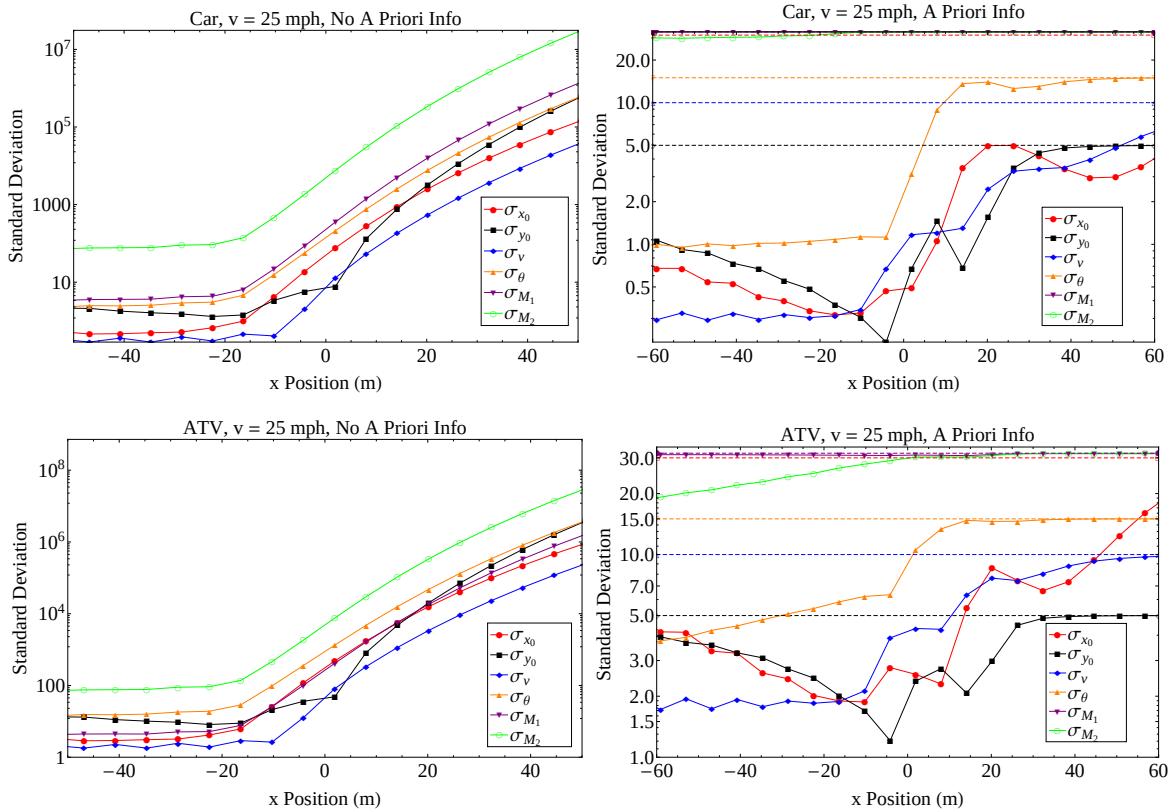

Figure 5: Variance versus position for the cases: no a priori information (left); a priori information (right)

evaluate magnetometers we are interested in identifying regions where the variances are above some threshold.

The Cramér-Rao bound can be used in other instances such as when a vehicle is passing a magnetometer with different speeds. Figure 6 is a log plot of the bounds on the standard deviation of the estimates for a single observation interval where the vehicle starts at the CPA. In both cases there is a singularity when the speed equals zero. With no a priori information, increases in speed result in substantial growth in variance so that estimation is no longer possible. In contrast, with a priori information,, there is a wider interval of velocities for which estimation may be possible.

6 Conclusions

The MITRE Corporation has developed a framework through which to estimate algorithm level Measures of Performance for a variety of surveillance scenarios. As part of that work, this analysis focuses on UGS utilizing of two-axis fluxgate magnetometers. Two MOPs are

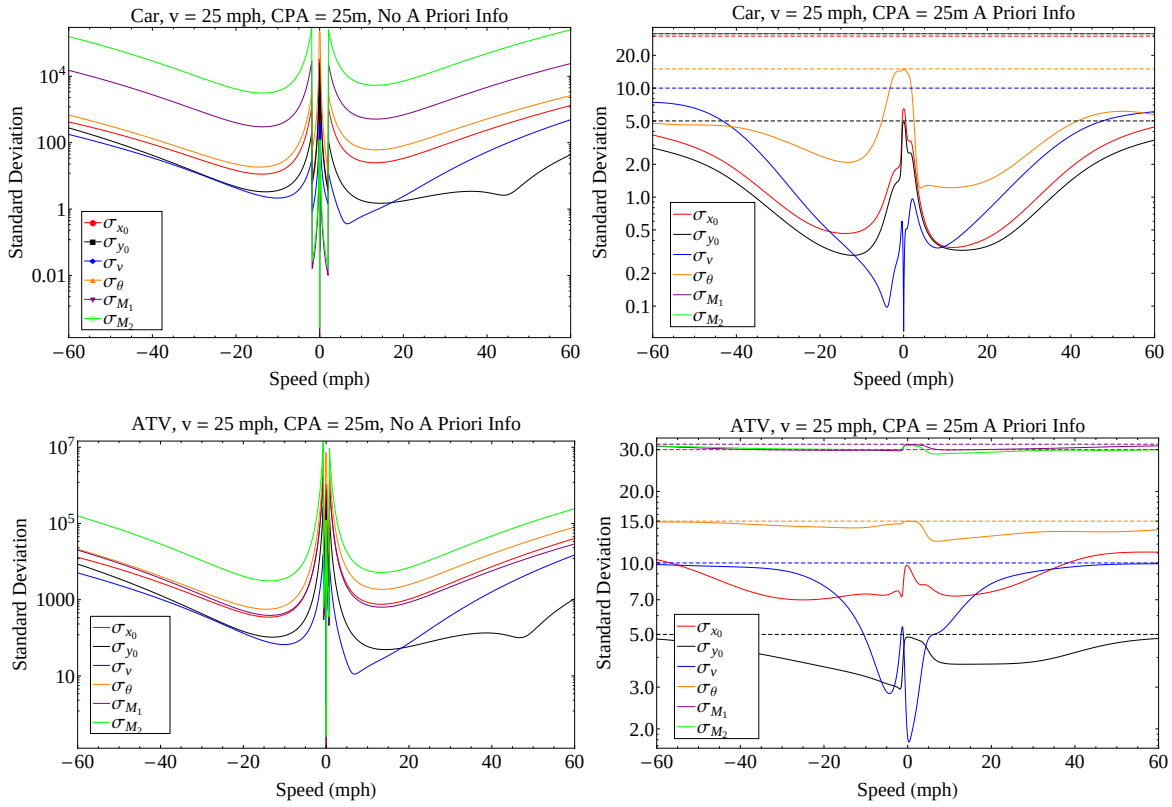

Figure 6: Variance versus speed for a car (top) and an ATV(bottom) starting from its closest point of arrival $(x_0, y_0) = (0, 25)$ for the cases where there is no a priori information (left) and where there is a priori information (right).

considered: the probability of detection and the Cramér-Rao bound for the variance of estimated parameters. A vehicle moving past a network of magnetometers is modeled as an ellipsoid and acts as a magnetic dipole. Assuming uniform linear motion over each observation period, the probability that a network of UGS detects the vehicle is calculated as a function of the vehicle, magnetometer, and location characteristics. We show that a series of sensors performs better than a single sensor and that the performance over a series of observation periods may be much greater than that of a single period. UGS may also be evaluated in terms of estimation ability. A lower bound on the variance of the vehicle's location, velocity and magnetic moments is computed for the cases where no a priori knowledge of the parameters exists as well as when the parameters are assumed to be Gaussian random variables with known variances. We show that UGS perform significantly better in the latter case and consider how vehicle speed affects estimation. An area for subsequent work is the development MOPs for a classification problem (i.e. classifying vehicles as heavy, medium size, or very light).

References

[1] J. E. Lenz. A review of magnetic sensors. *Proceedings of the IEEE*, 78(6):973–989, June 1990.

[2] E. M. Billingsley and S. W. Billingsley. Fluxgate magnetometers. *Proceedings of the IEEE*, 5090(194):194–203, 2003.

[3] C.T. Christou and G.M. Jacyna. Vehicle detection and localization using unattended ground magnetometer sensors. *Information Fusion (FUSION), 2010 13th Conference on*, pages 1–8, July 2010.

[4] Lionel Merlat and Pierre Naz. Magnetic localization and identification of vehicles. *Unattended Ground Sensor Technologies and Applications V*, 5090(1):174–185, 2003.

[5] J. A. Osborn. Demagnetizing factors of the general ellipsoid. *Phys. Rev.*, 67:351–357, Jun 1945.

[6] John D. Jackson. *Classical Electrodynamics Third Edition*. Wiley, third edition, August 1998.

[7] Robert N. McDonough and A. D. Whalen. *Detection of Signals in Noise*. Academic Press, Inc., Orlando, FL, USA, 2nd edition, 1995.

[8] John Meloy. What and where is the natural noise foor. http://www.vlf.it/naturalnoisefloor/naturalnoisefloor.htm, 2003.

Appendix

A. Vehicle Induced Moment

The induced moment for the vehicle may be written as

$$\mathbf{M} = VPH, \tag{A.1}$$

where $V = 4\pi AB^2/3$ is the volume of the ellipsoid, P is the magnetic polarizability tensor, and H is the earth's magnetic field strength rotated to the body axis frame of the vehicle.

To find P, let L_1 and L_2 be the demagnetization factors of the vehicle in the longitudinal and transverse directions. Then

$$L_1 = \frac{t_1}{c^2}, \quad L_2 = \frac{t_2 m}{2c^2}, \tag{A.2}$$

where

$$m = A/B, \qquad c = \sqrt{m^2 - 1}, \tag{A.3}$$

$$t_1 = \frac{m}{2c}\log\left(\frac{m+c}{m-c}\right) - 1, \quad t_2 = m - t_1 - 1. \tag{A.4}$$

The demagnetization factors are used to construct the magnetic polarizability tensor

$$P = \begin{pmatrix} \frac{\kappa}{1+\kappa L_1} & 0 & 0 \\ 0 & \frac{\kappa}{1+\kappa L_2} & 0 \\ 0 & 0 & \frac{\kappa}{1+\kappa L_2} \end{pmatrix} \tag{A.5}$$

where κ is the material magnetic susceptibility.

Now, to find H, let B_0 be the terrestrial magnetic induction, θ the vehicle's course with respect to true north, φ_i the magnetic inclination angle at the current location, and φ_d the magnetic declination angle at the current location. Then H is given by

$$H = \frac{2.5B_0}{\pi} \begin{pmatrix} \sin(\theta) & \cos(\theta) & 0 \\ -\cos(\theta) & \sin(\theta) & 0 \\ 0 & 0 & 1 \end{pmatrix} \begin{bmatrix} \sin(\varphi_d)\cos(\varphi_i) \\ \cos(\varphi_d)\cos(\varphi_i) \\ sin(\varphi_i) \end{bmatrix}. \tag{A.6}$$

The induced moment may now be written as

$$\mathbf{M} = VPH, \tag{A.7}$$

where $V = 4\pi AB^2/3$ is the volume of the ellipsoid[3].

B. Matched Filter Derivation

First consider the geomagnetic noise spectrum S_n that was derived in [8]. Let N_h be the noise spectral level in pTesla/sqrt(Hz) and f_ℓ be the frequency. The frequency is derived from the magnetometer sampling rate $F_s = 2B$, where B is the magnetometer bandwidth, and the observation time $T_{obs} = N/F_s$. The geometric noise spectrum may then be written as

$$S_n(f_\ell) = \frac{(10^{-12}N_h)^2}{f_\ell}. \tag{B.8}$$

Noise spectrum levels range from near 1 pTesla/sqrt(hz) in rural land areas, to greater than 100 pTesla/sqrt(Hz) in urban areas, and roughly 10 pTesla/sqrt(Hz) near water.

Next consider the sensor sensitivity noise spectrum, which we treat as quantization noise. Let Δ be the resolution of the device. Then, assuming the signal is uniformly distributed within a resolution cell, the variance can be shown to be[3]

$$\sigma^2 = \frac{\Delta^2}{12}. \tag{B.9}$$

The spectral density is flat and given by

$$S_s(f_l) = \frac{\Delta^2}{24B}; \qquad -B \le f_l \le B. \tag{B.10}$$

The combined noise spectrum is thus the sum of the sensor sensitivity spectrum and the background noise spectrum, $S_{noise} = S_n + S_s$.

A band pass filter is needed to remove the large terrestrial magnetic field component near DC as well as frequencies above the bandwidth of the sensor. This is implemented by removing frequencies less than F_{cut} and greater than B. Let $\tilde{B_1}$ and $\tilde{B_2}$ denote the band-passed filtered Fourier Transforms of the signals B_1 and B_2. The matched filter is then

$$d_1^2 = \frac{F_s}{N}\sum_{\ell=1}^{N}\frac{|\tilde{B}_1(f_l)|^2}{S_{noise}(f_l)} \tag{B.11}$$

$$d_2^2 = \frac{F_s}{N}\sum_{\ell=1}^{N}\frac{|\tilde{B}_2(f_l)|^2}{S_{noise}(f_l)} \tag{B.12}$$

from which the deflection ratio is[3]

$$d = \left(d_1^2 + d_2^2\right)^{\frac{1}{2}}. \tag{B.13}$$